IEEE Transactions on Automation Science and Engineering (T-ASE) paper, presented at ICRA 2026, Vienna, Austria.
Cite as T-ASE paper.

Towards Indirect Data-Driven Predictive Control for Heating Phase of Thermoforming Process

Hadi Hosseinionari, Mohammad Bajelani, *Graduate Student Member, IEEE* Klaske van Heusden, *Member, IEEE*
Abbas S. Milani, Rudolf Seethaler

***Abstract*—Shaping thermoplastic sheets into three-dimensional products is challenging since overheating results in failed manufactured parts and wasted material. To this end, we propose an indirect data-driven predictive control approach using Model Predictive Control capable of handling temperature constraints and heating-power saturation while delivering enhanced precision and overshoot control compared to state-of-the-art methods. We employ a Non-linear Auto-Regressive with Exogenous inputs model, which is linearized to define a linear control-oriented model at each operating point. Using a high-fidelity simulator, several simulation studies have been conducted to evaluate the proposed method's robustness and performance under parametric uncertainty, indicating overshoot and average steady-state error less than $2^{\circ}\mathrm{C}$ and $0.9^{\circ}\mathrm{C}$ ($7^{\circ}\mathrm{C}$ and $2^{\circ}\mathrm{C}$) for the nominal (worst-case) scenario. Finally, we applied the proposed method to a lab-scale thermoforming platform, resulting in a close response to the simulation analysis with overshoot and average steady-state error metrics of $5.3^{\circ}\mathrm{C}$ and $1^{\circ}\mathrm{C}$, respectively.**

***Note to Practitioners*—This work addresses a key challenge in the thermoforming process: precisely controlling sheet temperature during the heating phase to improve product quality and reduce waste. We present a data-driven control approach that can be implemented on existing thermoforming systems to enhance temperature accuracy and consistency. The proposed method uses historical process data to build a simplified model of heating dynamics. This model is then used in a predictive control framework to optimize real-time heater settings. The key advantages of the proposed method are improved temperature precision, faster settling times than conventional methods, the ability to handle practical constraints like maximum temperatures and heating power limits, and robustness to process variations and disturbances. Complex physics-based models or extensive system modifications are not needed. To implement this approach, practitioners would need to collect temperature and heater power data from their existing process, use it to train the data-driven model and integrate the control algorithm with their PLC or control system.**

***Index Terms*—Thermoforming, Thermal control, Manufacturing, Infrared Camera, NARX model, MPC.**

I. Introduction

COMPOSITE manufacturing has received considerable attention in Industry 5.0. More specifically, thermoplastic composites are increasingly used in the aerospace, marine, renewables, and automotive industries because of their thermomechanical properties and lightweight characteristics [1]. A thermoforming process involves applying heat and pressure to reshape flat plastic sheets [2], resulting in three-dimensional products. Fig. 1 shows a thermoforming setup with process sequences. The overall quality of the thermoformed product mainly depends on the heating phase's accuracy and the alignment of the heat distribution with the mold geometry. Temperature deviations can potentially result in undesired wrinkles and thickness [3]. Temperature control effectively helps reduce the number of rejected parts while minimizing cycle times and lowering the production cost. The main objective of this paper is a scalable solution to the heating phase control problem using data-driven techniques.

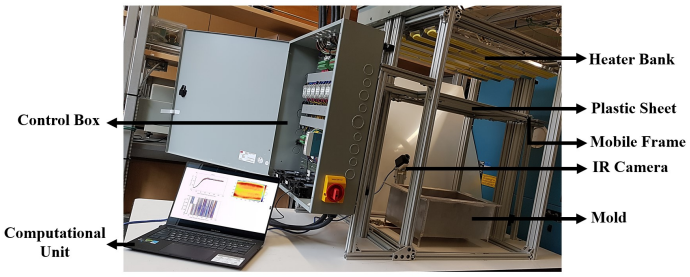

(a) Lab-scale thermoforming setup

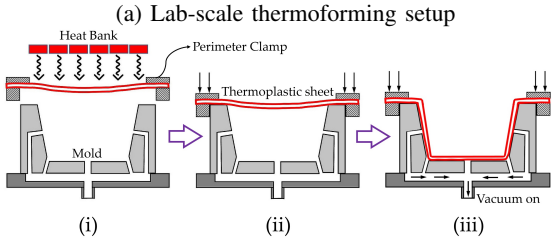

(b) Main sequences of a thermoforming process: (i) heating (ii) sealing or pre-stretch (iii) forming and cooling [4].

Fig. 1: An overview of a typical thermoforming process employed in this study.

Methods used in the thermoforming industry are limited to rule-based control laws that require expert knowledge or basic control strategies [5]. These traditional control methods cannot accommodate process constraints [6], including maximum and minimum temperature and heating/cooling rates that are critical for product quality. It has been shown that reducing the temperature disparity across the thickness of the sheet using model-based control improves product quality and reduces waste due to discarded parts [7]. In [8], a Model Predictive Control (MPC) solution was proposed for

Hadi Hosseinionari, Mohammad Bajelani, Klaske van Heusden, Abbas S. Milani, and Rudolf Seethaler are with the University of British Columbia, School of Engineering, 1137 Alumni Avenue, Kelowna, BC V1V 1V7 hadi.hosseinionari, mohammad.bajelani, klaske.vanheusden, abbas.milani, rudolf.seethaler @ubc.ca

the heating phase, which enables incorporation of process constraints. This solution used a physics-based model and requires full state measurements, which may not be available in an industrial setting. Evaluation of this controller was limited to a simulation study for the nominal case.

In industrial settings, there may be hundreds of heaters, resulting in a high-order and computationally expensive MPC solution. In addition, process uncertainty and model inaccuracies need to be accounted for. In [9], an approach combining MPC and Deep Reinforcement Learning (DRL) was introduced that addresses both the computational complexity of the controller and uncertainty in physics-based models. The trained agent performs similarly to Adaptive Model Predictive Control (AMPC) while reducing the computational load by a factor 14. The drawback of this method is that the offline training process increases with the number of heaters. A multi-agent transfer reinforcement learning framework for adaptive digital twinning of thermoforming heating systems was introduced in [10], demonstrating how learning-based control can enhance productivity while reducing energy consumption.

In [11], a multi-agent DRL approach was developed that only requires training of a single DRL agent by considering radiation from other heaters as a disturbance. This trained agent is subsequently deployed multiple times, each instance controlling a separate heater. The main limitation of this method is its dependency on the heater model: any change in the heater's model necessitates retraining the agent.

These solutions show that effective temperature control can improve product quality. However, these control solutions are not implementable at scale, as new settings require challenging and time-consuming modeling, or extensive data which is not available in industrial practice [12]. MPC's most challenging and time-consuming component is the prediction model [13], [14], [15]. This paper proposes a practical, data-efficient and scalable solution to control of the thermoforming process, aiming to provide a reliable and practical solution for industrial implementation. We propose a data-driven approach to obtain control-oriented reduced-order models for the thermoforming process. These reduced-order models are then used in a robustly tuned linear MPC, leading to a computationally efficient and robust control solution.

Thermoforming, like many control applications in manufacturing, exhibits nonlinear behavior combined with varying operational conditions. Application of data-driven modeling using Non-linear Auto-Regressive with Exogenous inputs (NARX) models combined with MPC has demonstrated potential for such systems [16], [17], [18], as well as for chemical systems [19], [20], [21] and thermal control [22]. NARX-MPC provides a balance between model complexity and prediction accuracy [23]. However, when using the complete NARX model, the resulting controller is nonlinear, leading to a nonconvex optimization problem and limited options for robustification. Recent work proposed stability-aware neural NARX formulations [24] that can match nonlinear MPC performance at reduced computational load. It does not address robustification with respect to model uncertainty.

In this paper, we propose a robust approach where we first identify a NARX model to ensure accurate representation of the nonlinear system behavior. We then linearize this NARX model at each operating point to obtain a linear control-oriented model, resulting in a data-efficient and easy-to-tune approach. This linearized model is used to design a linear MPC under MIMO constraints, including input constraint. By combining reduced-order control-oriented modeling, linear control and robust controller tuning, the resulting controller is robust to a range of process uncertainty and model mismatch due to both unmodeled dynamics and nonlinear behavior as shown in a simulation example. Experimental results show that the proposed solution can outperform more complex adaptive and learning control methods for this thermoforming process [9], [11]. Our results indicate that, in practice, a linear MPC using low-order control-oriented approximate model results in robust, high-performance control and simple implementation.

The subsequent sections of this paper are structured as follows: Section II details the high-fidelity model of the thermoforming system used in this study, the control objectives and the experimental setup. Section III describes the design methodology. Section IV specifies how this methodology is applied to the thermoforming system. Next, section V includes model validation, robustness analysis and discusses results obtained from the simulator and the real-world setup. Lastly, Section VI encapsulates the conclusions drawn from the study and outlines potential avenues for future research.

II. Background

A. High-fidelity Heat Transfer Model

This study uses a high-fidelity heat transfer model [4], which simulates the dynamics of a laboratory-scale thermoforming system. A brief overview is provided here, while more comprehensive details can be found in [4]. During the thermoforming process's heating phase, the primary heat transfer mode is from the heater bank to the sheet's surface through radiation. Depending on the material properties of the thermoplastic sheet, a fraction of the Infrared (IR) radiation is absorbed, leading to an increase in the temperature of the sheet. The thermoplastic sheet's elevated temperature results in heat dissipation to the environment through both convection and radiation. Additionally, assuming that the thermoplastic sheet is divided into $N_x \times N_y$ equal elements according to Fig. 2, conduction heat transfer occurs between adjacent elements on the thermoplastic sheet. The heat balance equation for each element on the sheet can be expressed as follows:

$$\rho V c_p \frac{\partial T_i}{\partial t} = \nabla \cdot (\overrightarrow{Q_{\mathrm{rad}}})_i + \nabla \cdot (\overrightarrow{Q_{\mathrm{conv}}})_i + \nabla \cdot (\overrightarrow{Q_{\mathrm{cond}}})_i. \quad (1)$$

In this equation, T_i is the temperature of ith element on the thermoplastic sheet. Q_{rad}, Q_{conv}, and Q_{cond} are radiation, convection, and conduction heat fluxes, respectively, ρ is the sheet material's density, V is the sheet element's volume, and $\mathrm{c_p}$ is specific heat. Radiation from the heater bank is the primary heat flux source toward elements on the thermoplastic sheet. The following equation represents this radiation heat flux.

$$Q_{\mathrm{rad}} = A_h \epsilon_e \sigma \sum_{i=1}^{N_x N_y} \sum_{h=1}^{H} F_{h \to i} (\theta_h^4 - T_i^4), \quad (2)$$

where A_h is the surface area of the heaters, ϵ_e shows the effective emissivity from heater to sheet, σ indicates the Stefan-Boltzmann constant, H is the number of heaters in the heater bank, $F_{h\to i}$ is the view factor between the h^{th} heater in the heater bank and the i^{th} element on the thermoplastic sheet, θ_h is the surface absolute temperature of the h^{th} heater in the heater bank, and T_i is the absolute temperature of the i^{th} element on the thermoplastic sheet. Heat dissipation to the surroundings occurs through radiation and convection heat transfer from the sheet elements. Notably, the convection heat transfer coefficient varies between the top and bottom faces of the sheet. Equation (3) delineates the convection heat flux from a sheet element to the environment.

$$Q_{\text{conv}} = (h_t + h_b)\Delta x \Delta y \Delta T, \tag{3}$$

where h_t and h_b represent the convection heat transfer coefficients at the top and bottom faces of the sheet, respectively, $\Delta x \Delta y$ denotes the surface area of the sheet element exposed to the air, and ΔT is the temperature difference between the sheet element and the ambient. Additionally, heat transfer through conduction occurs in adjacent elements from elements with higher temperatures to those with lower temperatures on the thermoplastic sheet. However, this type of heat transfer is relatively small compared to radiation and convection, owing to the low thermal conductivity of thermoplastic materials. Equation (4) details the conduction heat flux between sheet elements.

$$Q_{\text{cond}} = \mathrm{k} A_e \frac{\Delta T}{\Delta L}, \tag{4}$$

where k is the thermoplastic sheet material thermal conductivity, A_e is the element's cross-sectional surface area, ΔL is the width of the element in the x or y directions, and ΔT is the temperature difference between the ends. Figure 2 illustrates the heater bank alongside the thermoplastic sheet, partitioned into $N_x \times N_y$ equal elements. The figure delineates three types of heat transfer transpiring during the thermoforming heating phase. The region beneath each heating element on the thermoplastic sheet is called a "Zone". Every zone receives radiation from all heaters in the heater bank; however, the predominant infrared radiation received is from the heater directly above that specific zone. In the scenario where the sheet is discretized into cubic elements referred to as control volumes, equation (1) is integrated over each control volume and across the time interval from t to $t + \Delta t$. Hence, the temperature change in each sheet element is determined by the change in its internal energy, as expressed in equation (5).

$$T_{t+\Delta t} = T_t + (\frac{\Delta t}{\rho V c_p}) dU, \tag{5}$$

where $dU = Q_{\text{rad}} + Q_{\text{conv}} + Q_{\text{cond}}$.

This model is nonlinear and a high-order approximation of the infinite dimensional heat transfer process.

B. Control Objectives for Thermoforming Systems

Our main objectives for controlling the heating phase of thermoforming systems are efficiency, reliability, and scalability.

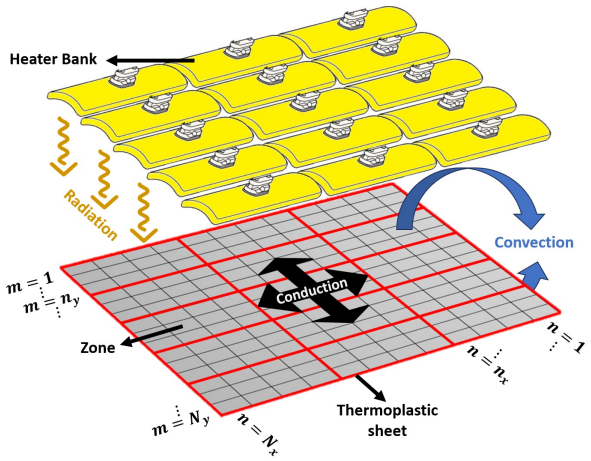

Fig. 2: Thermoplastic sheet meshing and definition of the zone.

1) Heating beyond Glass Transition Temperature: One of the critical control objectives is the handling of overheating (temperature overshoot). From a thermo-mechanical perspective, the appeal of amorphous thermoplastics lies in their wide forming window, which stems from their rubber-like behavior. This behavior occurs above the glass transition temperature T_g and extends over various temperatures. The thermoformability of these materials hinges on finding a balance between withstanding significant deformations and maintaining a certain level of rigidity to prevent excessive sheet flow during heating. Typically, the forming window ranges from 30 to 60 °C above T_g for most amorphous thermoplastics [25]. The overshoot should be carefully controlled so the thermoforming processes do not exceed the forming window of the material. This constraint is essential to prevent material degradation and ensure product quality. Consequently, the admissible set, $\mathcal{Y}$ is defined as follows:

$$\mathcal{Y} = \{\mathcal{T}_i | i \in \{1, ..., 15\}, \mathcal{T}_i - \mathcal{T}_i^r \leq \mathcal{T}_{over}\}, \tag{6}$$

where $\mathcal{T}_i$ and $\mathcal{T}_i^r$ are each zone's average and reference temperature on the thermoplastic sheet, respectively. $\mathcal{T}_{over}$ denotes the allowable overshoot temperature determined by the material properties, which is considered equal to zero in this paper.

2) Operating Time Efficiency: To enhance production efficiency, the control system must minimize the rise time and settling time during the heating phase. A rapid and accurate approach to the desired temperature setpoint, without excessive overshoot, is essential for increasing throughput.

3) Minimizing the error at the end of the heating phase: To maintain precise temperature control and ensure product quality, the control system must minimize the error between the desired temperature and the temperature achieved at the end of the heating phase.

4) Robustness: Industrial environments present numerous challenges, including variations in system parameters such as ambient temperature, which can affect the thermoforming process. The gap between the heater bank and the thermoplastic sheet is one of the most important system parameters. A smaller gap reduces disturbance from neighboring heaters,

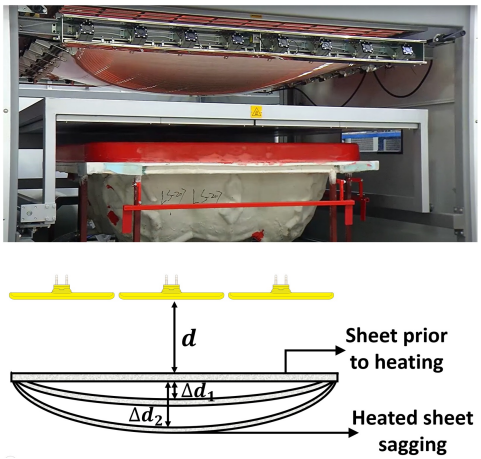

Fig. 3: An industrial example of large sheet sagging during the heating phase: CMS plastic technology company [26]

resulting in system behavior similar to a Single-Input Single-Output (SISO) configuration for each zone. In contrast, this minor gap may form hot spots on the thermoplastic sheet, disrupting the desired smooth temperature distribution. During the heating phase, high temperatures cause the large sheets to lose their structural integrity and sag downwards under their weight; see Fig. 3. This sagging leads to different gaps between heaters in the heat bank and their associated zones during the heating phase. The proposed method must be robust to sensitive system parameters, maintaining optimal control performance despite external disturbances. This robustness is crucial for ensuring consistent process outcomes and minimizing the need for manual adjustments.

5) Scalability: Another aspect is the control system's scalability, especially in industrial settings where thermoforming processes may involve hundreds of heaters. All aspects of the controller design need to be scalable to a high number of inputs and output zones, from modeling to control implementation and computational load.

C. Experimental Setup

The physical setup illustrated in Fig. 1a is a lab-scale thermoforming system with fifteen ceramic heating elements (FTE-500, Ceramicx Company) arranged in five rows and three columns in the heater bank. Each zone receives radiation from all heaters in the heater bank, indicating a Multi-Input Multi-Output (MIMO) system. A mobile frame holds the thermoplastic sheet during the heating phase and transfers it to the mold once the heating phase is completed. A FLIR Infrared (IR) camera (FLIR A35) provides temperature feedback from the thermoplastic sheet's surface to the control algorithm with a 60 Hz frame rate and 16-bit video streaming. The compact dimensions of the thermal camera (29 × 36 × 59 mm) enhance its versatility within the experimental setup. Control input values are transmitted to an Arduino Atmega 2560 via a serial port, where they are processed to manage the states of the relays (Omega - SSRL240AC10). The input values, derived from MATLAB and representing the output of the control algorithm within the range of 0 to 255 units, are used by the Arduino firmware to generate PWM signals. The AC unit is segregated into two circuits to manage the power requirements. The first circuit powers eight heaters, each drawing 2.5 Amps, while the second circuit caters to seven heaters with the same power draw. Each unit operates within a range of 220V and up to 20 Amps. Table I shows this study's model parameters.

TABLE I: System parameters.

Parameter	Description	Values	Unit
ρ	sheet density	1380	$\left[\frac{\text{kg}}{\text{m}^3}\right]$
c_p	specific heat capacity	1465	$\left[\frac{\text{J}}{\text{kg}\cdot\text{K}}\right]$
ϵ_e	effective emissivity	0.95	-
k	material thermal conductivity	0.18	$\left[\frac{\text{W}}{\text{m}\cdot\text{K}}\right]$
h	convection heat transfer coefficient	5	$\left[\frac{\text{W}}{\text{m}^2\cdot\text{K}}\right]$
Δz	sheet thickness	0.002	[m]
L_x	sheet length	0.75	[m]
L_y	sheet width	0.5	[m]

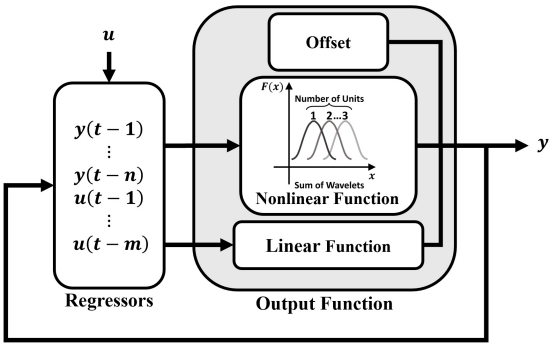

Fig. 4: A single-output NARX model block diagram.

III. Methodology: Data-Driven System Modeling and Predictive Control

To meet the reliability, efficiency and scalability specifications, we propose an indirect data-driven approach. In the first step, a low-order nonlinear model with NARX structure is identified from data. This model is then validated for the range of operating points that is captured by the data. In the next step, the validated model is linearized for the operating point of interest. This linearized model is then used to design a robustly tuned MPC controller.

The methods used in this work are described below in Section III. Section IV describes how this methodology is applied to the thermoforming system, including experiment design, the approach to model validation and the MPC design choices. Results of the model validation, critical to the validity of the proposed approach, are included in Section V.

A. Data-Driven System Modeling: Nonlinear Autoregressive Exogenous (NARX)

A NARX model extends the traditional linear ARX structure by incorporating linear and nonlinear components in parallel; see Fig. 4. It consists of two main components: a regressor vector and an output function. The regressor vector contains past input-output data, indicating the model's order. The

output function involves offset, nonlinear, and linear functions, indicating the model's structure. Since the output function benefits from a parallel structure, its nonlinear and offset parts are dedicated to reducing the modeling error that cannot be captured by the linear part. A NARX model with a wavelet nonlinear function can be represented as follows:

$$X_t = \left[\ y_{[t-1:t-n]}, u_{[t-1:t-m]}\ \right]^\top, \tag{7a}$$

$$y_t(X_t) = X_t^T PL + W(X_t) + S(X_t) + \varepsilon, \tag{7b}$$

where $X_t \in \mathbb{R}^{(n+m)\times 1}$ the regressor vector at time step t, ε is the offset, $P \in \mathbb{R}^{(n+m)\times p}$ is a projection matrix, transforming the regressors into a lower-dimensional space, $L \in \mathbb{R}^{p\times 1}$ is linear mapping that scales the projected regressors to the output. $W(X_t)$ represents the sum of dilated and translated wavelets, which are functions that capture the localized features of the signal. $S(X_t)$ represents the sum of dilated and translated scaling functions, also known as scales, which capture the global trends of the signal. The functions $W(X_t)$ and $S(X_t)$ together form the wavelet network's nonlinear component, allowing the NARX model to approximate complex, nonlinear relationships between the inputs and outputs [27]. To linearize the NARX model, consider the following equation:

$$X_{t+1} = AX_t + [B_1\ B_2]\begin{bmatrix} y_t \\ u_t \end{bmatrix}, \tag{8a}$$

$$y_t = \mathcal{F}(X_t, u_t), \tag{8b}$$

where $\mathcal{F}$ is a nonlinear function representing the output function in Figure 4. X_t and u_t are state and the input vectors at time t, respectively.

To establish a linear state-space model around the operating point $y_{op} = \mathcal{F}(X_{op}, u_{op})$, the first derivatives of the function $\mathcal{F}$ with respect to the state vector X and the input u are represented as follows:

$$\mathcal{F}_X = \frac{\partial}{\partial X}\mathcal{F}(X,u)\Big|_{\substack{u=u_{op}\\X=X_{op}}}, \quad \mathcal{F}_u = \frac{\partial}{\partial u}\mathcal{F}(X,u)\Big|_{\substack{u=u_{op}\\X=X_{op}}}, \tag{9}$$

Using the derivatives, the changes in the output and state vector from their values at the operating point can be approximated by the following linear equations:

$$\Delta X_{t+1} = A\Delta X_t + [B_1\ B_2]\begin{bmatrix} \Delta y_t \\ \Delta u_t \end{bmatrix}. \tag{10a}$$

$$\Delta y_t = \mathcal{F}_X \Delta X_t + \mathcal{F}_u \Delta u_t. \tag{10b}$$

By substituting equation (10b) in (10a), the linear approximation for the state vector around the operational point is defined as follows:

$$\Delta X_{t+1} = (A + B_1\mathcal{F}_X)\Delta X_t + (B_1\mathcal{F}_u + B_2)\Delta u_t, \tag{11}$$

where $\Delta X_t = X_t - X_{op}$, $\Delta u_t = u_t - u_{op}$, $\Delta y_t = y_t - y_{op}$ are the deviation of the state vector, input, and output from their value at the operating point, respectively. B_1 and B_2 are matrices that relate the input and the output to the state changes. This method is implemented by the "linearize" command in MATLAB® - System Identification Toolbox.

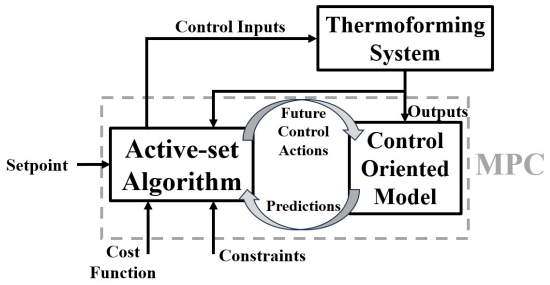

Fig. 5: MPC block diagram [9].

B. Model Predictive Control (MPC)

MPC is an advanced control technique that enables solving a constrained finite horizon optimal control problem, with the cost of solving an on-the-fly optimization problem. As an optimization-based controller, MPC can systematically handle input-output constraints [28], [29]. One of the challenges in implementing MPC in industrial settings is the need for sufficiently accurate system models [30]. Often, highly accurate and over-complicated models may not be suitable for control design as the underlying optimization problem becomes expensive and time-consuming, especially for high-dimensional systems. In this work, we propose to use a low-order *control-oriented* model that is obtained by linearizing the NARX model, following (10a-10b). For a servo-tracking problem[1], we define the MPC problem as follows:

$$\begin{aligned} \underset{u}{\text{minimize}} \quad & \textstyle\sum_{t=1}^{N_p} \alpha e_t^T e_t + \sum_{t=0}^{N_c-1} \beta \Delta u_t^T \Delta u_t \\ \text{subject to} \quad & X_{t+1} = \mathcal{A}X_t + \mathcal{B}u_t, \\ & y_t = \mathcal{C}X_t + \mathcal{D}u_t, \\ & e_t = r - y_t, \\ & y_t \in \mathcal{Y}, u_t \in \mathcal{U}, \end{aligned} \tag{12}$$

where α and β penalize the tracking error and rate of the control inputs, $\mathcal{U}$ and $\mathcal{Y}$ are admissible sets for inputs and outputs, ensuring the system operates within safe and efficient bounds, $\mathcal{A} = A + B_1\mathcal{F}_X$, $\mathcal{B} = B_1\mathcal{F}_u + B_2$, $\mathcal{C} = \mathcal{F}_X$ and $\mathcal{D} = \mathcal{F}_u$ are the matrices of the control-oriented model from (10a). N_p and N_c are the prediction and control horizons, respectively. Δu_t is the increment of control input at time step t, required to eliminate steady state errors. The general architecture of the proposed method is depicted in Fig. 5.

IV. Proposed Control Strategy for Thermoforming System

This section specifies the proposed indirect modeling and MPC method as applied to the lab-scale thermoforming system, and details how the modeling phase and control law were designed to meet the control objectives.

A. Data-driven modeling for Thermoforming System

Experiment design[2] for nonlinear systems requires physical understanding of the system, as the required excitation depends

[1]The reference, r_t, is a constant signal over the prediction horizon.
[2]Data collection for SysID purposes.

on the nonlinearity, in addition to mathematical conditions such as persistently exciting (PE) inputs that are required for linear systems [31]. For a thermoforming system, we outline an experiment to collect data for modeling purposes with the following criteria: I) The input should drive the system across a broad range of sheet temperatures to expose the non-linearity of the system. II) The system's output should oscillate around various equilibrium points to capture the system's gain characteristics. III) Given the distinct nonlinear behaviors during thermoforming systems' warming and cooling phases, the input signal must be designed to explore these phases comprehensively. The system's non-linearity is gain-dependent and mainly depends on sheet temperature.

To meet these requirements, we employ a pseudo-random binary sequence (PRBS) signal with the upper and lower bounds increasing every 200 minutes with the amplitude of $100\,[\mathrm{W}]$ until reaching a maximum of $500\,[\mathrm{W}]$, after which it decreases similarly.

The validated physics-based model described in Section II-A was used to generate a simulated data set. A measurement noise signal, sampled from a standard normal distribution, was added to the measurements. Use of this artificial data-set enables evaluation of robustness and performance in simulation, required to establish whether the proposed method meets the objectives.

Parameter estimation is carried out using MATLAB® - System Identification Toolbox to achieve the best parameters in the NARX model, considering 15 Wavelet networks. The optimal accuracy of the model, smallest NRMSE, is observed when parameters n and m in the regressor vector related to the number of past inputs and outputs are set to 2. The accuracy of the model is evaluated based on NRMSE and correlation analysis criteria on the test data. Furthermore, the dataset is split into train and test subsets, comprising 75% and 25% of the data, respectively.

B. Proposed MPC for Thermoforming System

We linearize the identified NARX model for the target operating conditions and design a linear MPC using this linearized model. By design, using this linear control-oriented model in MPC demands fewer computational resources than a full high-order physics-based model, thus making it more scalable for real-time control in industrial settings. Each zone is modeled with a succinct set of regressors and the MPC is implemented by solving a Quadratic Programming (QP) problem. This scalability ensures that the control strategy can be efficiently applied across different machines and setups, facilitating its adoption in diverse industrial environments.

The model inputs encompass the electrical power of the heaters within the heater bank, u, and the outputs comprise the average temperature of each zone on the thermoplastic sheet, $\mathcal{T}$. Equation (13) shows the regressor vector for the NARX model proposed for thermoforming systems.

$$X_t = \begin{bmatrix} \mathcal{T}_{t-1:t-n} \\ u_{t-1:t-m} \end{bmatrix}, \tag{13}$$

where $\mathcal{T}_{t-1:t-n} \in \mathbb{R}^{Z\times n}$ and $u_{t-1:t-m} \in \mathbb{R}^{H\times m}$ are the past n and m output and inputs at discrete-time index t, respectively (see also equation 7a). Z is the total number of zones on the thermoplastics, and H shows the number of heaters. The system's input (heater's power) and output (sheet's temperature) u_{t-n} and $\mathcal{T}_{t-n}$, respectively, at time step $t-n$ take the following form:

$$\mathcal{T}_{t-n} = \begin{bmatrix} {\mathcal{T}_{t-n}}^{(1)} \\ {\mathcal{T}_{t-n}}^{(2)} \\ \vdots \\ {\mathcal{T}_{t-n}}^{(Z)} \end{bmatrix}, u_{t-n} = \begin{bmatrix} {u_{t-n}}^{(1)} \\ {u_{t-n}}^{(2)} \\ \vdots \\ {u_{t-n}}^{(H)} \end{bmatrix}. \tag{14}$$

The range of values $u^{(1)}, \cdots, u^{(H)}$ are from 0 to 500 W, indicating the minimum and maximum power levels that are applied to each heater, indicating input admissible set $\mathcal{U}$ in equation 12.

To meet the specifications, in particular 2) and 4) (efficiency and robustness), the controller is tuned to provide aggressive yet safe control actions, which is achieved by setting a higher value for α compared to β in equation (12).

Limiting the control error at the end of the heating phase (specification 3)) is achieved by the use of a terminal error at the end of each control horizon. Specifically, the absolute difference between the desired set-point temperature and the actual temperature of each zone should be less than the required control accuracy, which is considered 5 °C in this study. This constraint can be expressed as:

$$|\mathcal{T}_i(t_f) - \mathcal{T}_i^r| \leq 5^{\circ}\mathrm{C}, \quad \forall i \in 1, \ldots, 15 \tag{15}$$

where t_f denotes the end of the control horizon, and $\mathcal{T}_i(t_f)$ represents the actual temperature of zone i at time t_f. Enforcing this terminal error constraint ensures that the temperature distribution across the thermoplastic sheet is within an acceptable tolerance range, preventing material degradation and maintaining consistent product quality.

V. Results

This section includes validation of the NARX model, evaluation of the robustness and performance of the proposed controller using the simulation environment, and experimental implementation. In simulation, performance of the proposed controller is compared to three state-of-the-art methods: MPC-guided Deep Reinforcement Learning (DRL), Adaptive MPC (AMPC) [9], and Multi-agent DRL [11]. Next, the proposed method's robustness against three important system parameters, convection heat transfer coefficient (h), the gap between the heater bank and the thermoplastic sheet (d), and the radiation absorptivity of the thermoplastic sheet (α) are examined. Finally, the lab-scale experimental thermoforming setup is used to verify the proposed control algorithm as a physical platform and the experimental results compared to the multi-agent DRL in [11].

A. Model Validation

The (nonlinear) NARX model was validated by 1) evaluating the fit to data of the one-step-ahead predictor, 2) auto- and cross-correlation tests and 3) evaluating the N-step ahead

TABLE II: Accuracy of the proposed NARX model for the test data in the closed-loop simulation: NRMSE for each zone versus N-step prediction horizon (percentage).

N	1	10	30	50	80	100
Zone 1	98.58	97.59	94.41	91.47	87.78	85.73
Zone 2	98.59	97.46	93.97	90.74	86.68	84.44
Zone 3	98.49	97.39	93.89	90.68	86.65	84.43
Zone 4	98.61	97.48	93.99	90.80	86.77	84.54
Zone 5	98.61	97.34	93.51	90.02	85.62	83.19
Zone 6	98.57	97.32	93.52	90.05	85.67	83.24
Zone 7	98.60	97.39	93.77	90.47	86.34	84.06
Zone 8	98.62	97.24	93.22	89.57	84.99	82.46
Zone 9	98.55	97.25	93.35	89.77	85.26	82.75
Zone 10	98.58	97.44	93.92	90.68	86.60	84.35
Zone 11	98.60	97.28	93.33	89.74	85.24	82.76
Zone 12	98.58	97.34	93.61	90.21	85.93	83.56
Zone 13	98.51	97.49	94.23	91.21	87.42	85.34
Zone 14	98.52	97.33	93.62	90.21	85.94	83.59
Zone 15	98.49	97.43	94.06	90.98	87.12	85.01

prediction accuracy. The model was validated for all zones. For readability, results are presented for a representative zone.

Input and output data as well as the 1-step ahead prediction and prediction error for Zone 1 are shown in Fig.6. The model fit is adequate, with an error of less than 5 degrees over a temperature range of over 400 degrees.

Fig.7 (first subplot) presents the sample autocorrelation of the residuals for Zone 1. The sharp central peak and the fact that most values remain within the 99% confidence bounds suggest that the identified model has captured the dominant dynamics, with residuals primarily reflecting measurement noise. The second subplot in Fig.7 displays the sample cross-correlation between the residuals and lagged inputs for Zone 1. The low correlation values, largely confined within the 99% confidence interval, indicate that the model has effectively utilized the information available in past inputs. Note that the cross-correlation does not align with a stochastic error, and can be attributed to unmodeled nonlinear effects. Minor excursions beyond the confidence bounds in the autocorrelation Fig.7 (top) can also be attributed to unmodeled nonlinear effects. The model captures most, but not all of the nonlinearity of the system.

In addition to these validation tests, we evaluated the accuracy of N-step ahead predictions. The model was identified using 1-step ahead predictions. However, the model will be used in MPC, where multiple steps are predicted. The accuracy of such multi-step-ahead predictions can degrade due to the accumulation of one-step-ahead prediction errors during model recursion. To assess the accuracy and robustness of the NARX model's multi-step-ahead predictions, N-step ahead predictions were also evaluated against the test set. The model's accuracy is quantified by the Normalized Root Mean Square Error (NRMSE) and presented in Table II.

$$\text{NRMSE} = \frac{\sqrt{\frac{1}{N_d}\sum_{i=1}^{N_d}(y_i - \hat{y}_i)^2}}{\max(y) - \min(y)}, \tag{16}$$

where N_d is the number of data points, y is the noise-polluted measurement, and $\hat{y}$ is the model's predicted output.

Table II presents the model's accuracy for each zone relative to the prediction horizon for test data, which was the final 25% of the entire data set. For the prediction horizon of 100 steps, the model's accuracy is more than 80% on the test dataset. The (nonlinear) NARX model is validated for the range of operating conditions represented in the data, and adequate for controller design for target operating conditions within this range.

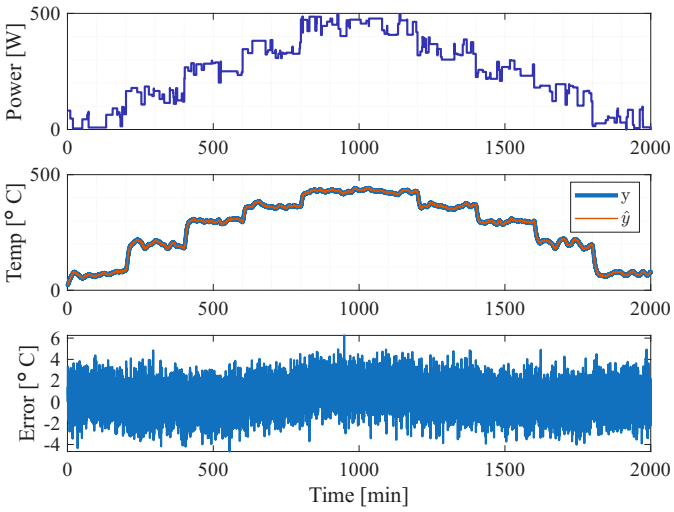

Fig. 6: Top: Input excitation signal applied to the first heater during data collection. Middle: Measured output and the NARX model's one-step-ahead prediction for Zone 1. Bottom: Corresponding one-step-ahead prediction error.

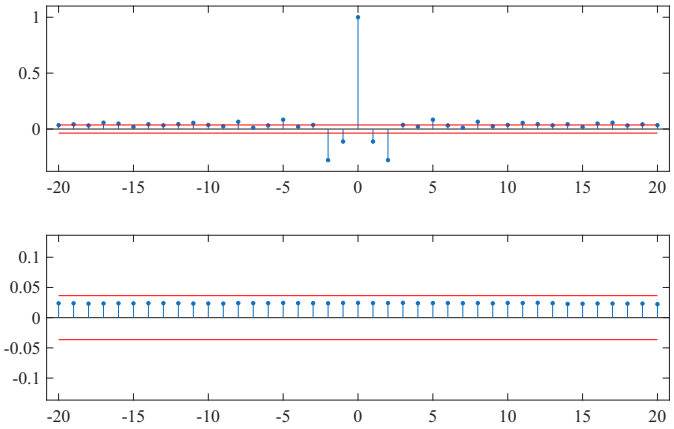

Fig. 7: Autocorrelation of the residual e_1 (top) and cross-correlation between the input u_1 and residual e_1 (bottom) for Zone 1 on the test dataset. The red bounds indicate the 99% confidence interval.

B. Controller Evaluation: Numerical Results

To evaluate the controller's performance in various settings and conduct a comparative analysis with AMPC, MPC-guided DRL, and multi-agent DRL the same base scenario introduced in [9] and [11] is considered. Table III shows the reference temperature distribution used in the comparisons.

1) Comparison Study: The following performance metrics for comparison are considered: the average and the maximum error of zones at the end of the simulation time, the maximum

TABLE III: Desired temperature distribution on the simulator and experimental implementation.

Zone	Ref. Temp. Sim. [°C]	Ref. Temp. Exp. [°C]	Zone	Ref. Temp. Sim. [°C]	Ref. Temp. Exp. [°C]	Zone	Ref. Temp. Sim. [°C]	Ref. Temp. Exp. [°C]
1	165.5	83	6	117	55	11	129.8	71
2	130.3	66	7	165.4	85	12	117.1	54
3	118.2	51	8	125.5	75	13	167	83
4	167.5	84	9	114.8	56	14	136.3	66
5	127.6	70	10	166.9	85	15	119.7	53

overshoot, and the settling time within an error bound of $\pm 10°\mathrm{C}$. Figure 8a shows the error variation across the 15 zones on the thermoplastic sheet over the simulation time. After 560 seconds, the error signals lie in the $\pm 10°\mathrm{C}$ bound. The maximum overshoot and the average (maximum) error of zones are $2°\mathrm{C}$ and $0.7°\mathrm{C}$ ($1.4°\mathrm{C}$), respectively. Also, Fig. 8b indicates the control inputs applied to 15 heaters bounded in $[0, 500]$ Watts.

Table IV compares the performance of the proposed method with AMPC, MPC-guided DRL, and multi-agent DRL across seven criteria on the simulator. AMPC requires feedback from the surface temperature of heaters since it uses a linearized physics-based system model around operational points. In contrast, MPC-guided DRL, multi-agent DRL, and the proposed method are developed based on input (heaters' heating power) and output (zone temperatures) measurements. With an increase in the heaters in the heater bank, the system's inputs and outputs also increase, leading to higher complexity in the models utilized by the centralized MPC methods and, consequently, longer online computational time. However, while this complexity affects the offline training time of MPC-guided DRL, its online computational time remains low once trained, enabling fast operation. Furthermore, in multi-agent DRL, each heating element is assigned its own agent. Consequently, any modifications to the heater bank layout have no impact on the online or offline computational time. Concerning accuracy, although the proposed method performs comparably to multi-agent DRL, it surpasses both AMPC and MPC-guided DRL by achieving a notably tighter final error bound. In particular, the proposed method's error bound is 3.5 times narrower than AMPC's and 5.5 times narrower than MPC-guided DRL's.

Using the proposed method substantially reduces the overshoot, decreasing from $12°\mathrm{C}$ in AMPC and MPC-guided DRL and $6°\mathrm{C}$ in multi-agent DRL to $2°\mathrm{C}$. This represents a significant reduction in overshoot. Furthermore, concerning settling time within an error bound of $\pm 10°\mathrm{C}$, the proposed MPC can achieve this error bound in 560 seconds. In contrast, the settling times for the AMPC and MPC-guided DRL methods are 650 seconds and 765 seconds, respectively.

2) Robustness Analysis: This section assesses the robustness of the proposed method by examining its sensitivity to a wide range of variation in three critical system parameters: convection heat transfer coefficient (h), the gap between the heater bank and the thermoplastic sheet (d), and the radiation absorptivity of the thermoplastic sheet (α). This analysis enables us to assess the robustness of the proposed method before implementing it on the real-world setup in section V-C. The proposed method's performance is evaluated based on the maximum overshoot and final average error across zones for different mentioned parameters. The nominal condition is defined as $h = 5[\frac{W}{m^2}]$, $d = 15[\mathrm{cm}]$, and $\alpha = 0.8$.

In Figure 9a and Figure 9b, the heat transfer coefficient was varied for different distances between the sheet and the heaters while keeping the absorptivity at 0.8. In Figure 9c and Figure 9d, the heat transfer coefficient was varied for different absorptivity coefficients while keeping the distance between the heater bank and the sheet at 15 cm. Figure 9a and Figure 9c collectively indicate that the proposed MPC is robust to significant variations in parameters. It consistently maintains the average error of zones on the sheet below 2 °C after the control process. Furthermore, as illustrated in Figure 9b, an increase in the distance between the heater bank and the sheet results in a larger overshoot. This outcome is logical, given that the heater's radiation pattern covers a broader area on the sheet, potentially impacting other zones as a disturbance. Additionally, Figure 9 demonstrates that an elevation in the convection heat transfer coefficient (due to a drop in room temperature or exposure of the sheet to wind) leads to a decrease in both maximum overshoot and the final accuracy. The outcomes depicted in Figure 9 indicate the proposed MPC is robust in handling disturbances introduced by changes in system parameters.

C. Controller Evaluation: Experimental Results

The practical application of the proposed method is evaluated on the experimental thermoforming setup, detailed in section II-C. The controller designed using the high fidelity simulator was implemented and evaluated. A feasible non-uniform reference temperature distribution from [11] is chosen to evaluate the controller's performance, as shown in table III, given the ambient temperature during the experimental test equal to $21°\mathrm{C}$. Fig. 10 illustrates the system's output, measured temperature profile on the thermoplastic sheet by IR camera, at time stamps $t = 100[\mathrm{sec}]$, $t = 200\,[\mathrm{sec}]$, and $t = 900\,[\mathrm{sec}]$. Figure 10d depicts the error variation across the 15 zones on the thermoplastic sheet. It shows that the controller effectively reduces the error of zones within the ± 10 bound after 308 seconds, with the average and maximum error of zones at the control process's conclusion being approximately $1°\mathrm{C}$ and $3.8°\mathrm{C}$, respectively, and the maximum overshoot equal to $5.3°\mathrm{C}$. Additionally, Fig. 10e indicates the control inputs applied to the 15 heating elements.

Table V compares the proposed MPC controller's performance for the same reference temperature distribution on a physics-based simulator and a real-world lab-scale thermoforming setup. The results indicate a close alignment in performance when subjected to an identical reference temperature distribution on both platforms. Notably, the settling time within the experiment's error bound of $\pm 10°\mathrm{C}$ was recorded as 308 sec, shorter than the simulator's settling time. Also, the overshoot on the real-world setup is almost $5°\mathrm{C}$ higher than the simulator. This disparity suggests differences in system parameters between the simulator and the experiment. For

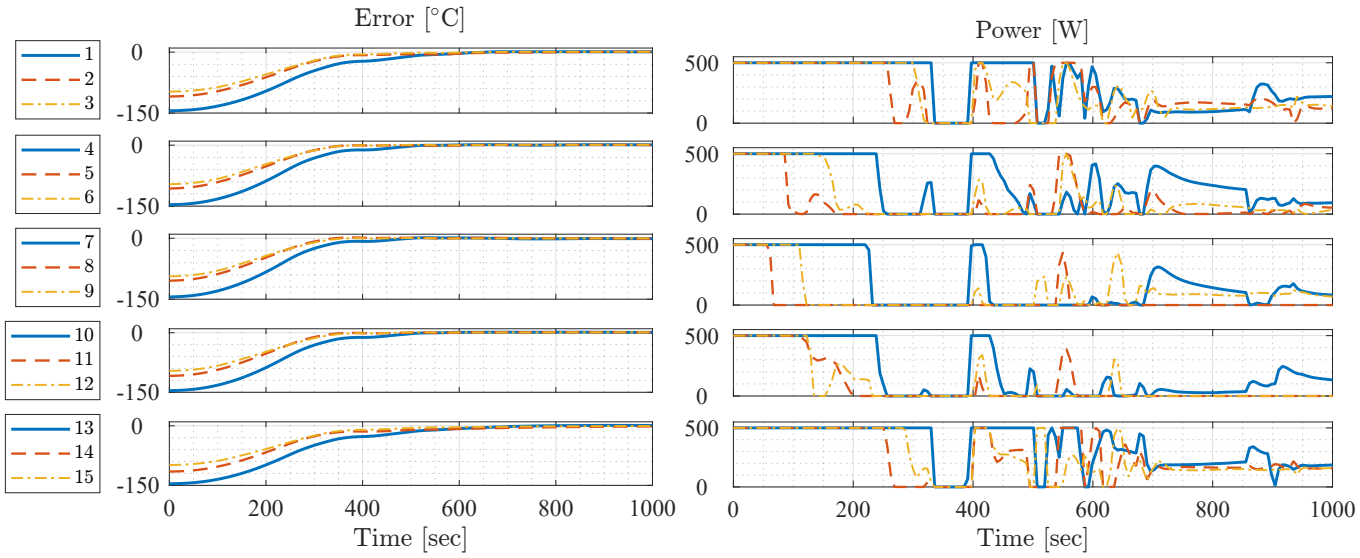

Fig. 8: Simulation results of the proposed method applied on the physics-based simulator (H denotes each heater, and Z denotes each zone). (a) error signals for the nonuniform reference temperature distribution. (b) input signals for the nonuniform reference temperature distribution.

TABLE IV: A comparison between AMPC, MPC-guided DRL, and proposed MPC using linearized NARX model on the physics-based simulator.

Metric	AMPC	MPC-guided DRL	Multi-agent DRL	Proposed MPC with Linearized NARX Model
Reliance on model	D&I	Training	Training	D&I
Requires heater temp. bank's feedback	Yes	No	No	No
Average online comp. time [ms]	921	11	11	90
Average error after 1000 sec [°C]	1.5	1.8	**0.3**	0.7
Maximum error after 1000 sec [°C]	±5	±8	**±1**	±1.4
Maximum overshoot [°C]	12.0	11.8	6	**2.0**
Settling time [sec]	650	765	**350**	560

D: Design I: Implementation

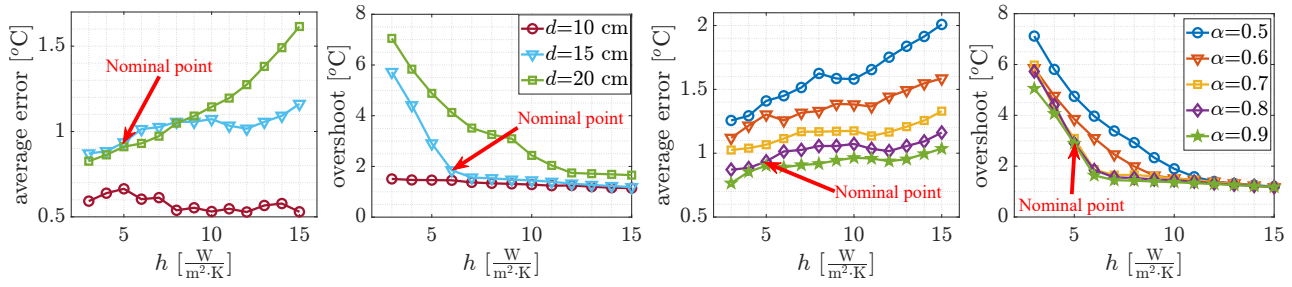

Fig. 9: Robustness evaluation: (a) The average error of zones under varying convection heat transfer coefficients and gaps between the heater bank and the sheet. (b) Maximum overshoot under varying convection heat transfer coefficients and gaps between the heater bank and the sheet. (c) The average error of zones under varying convection heat transfer coefficients and sheet absorptivity coefficients. (d) Maximum overshoot under varying convection heat transfer coefficients and sheet absorptivity coefficients.

instance, variations may arise if the convection heat transfer coefficient in the lab is lower than that considered in the simulator or if the sheet's radiation absorptivity is higher than the simulated values.

Table VI compares the proposed MPC controller with the multi-agent DRL approach on the real-world lab-scale thermoforming setup described in Section II-C. As shown, the proposed MPC achieves slightly improved accuracy, with average and maximum errors of 1°C and 3.8°C, respectively. Moreover, the overshoot is nearly halved, dropping from

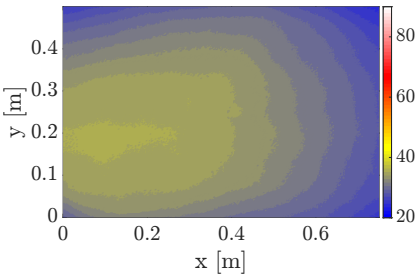

(a) Temp. distribution at $t = 100\,[sec]$

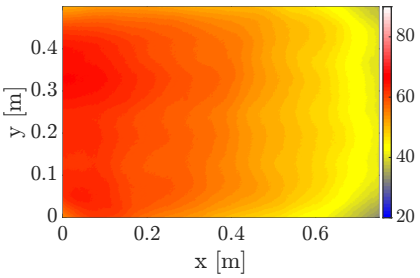

(b) Temp. distribution at $t = 200\,[sec]$

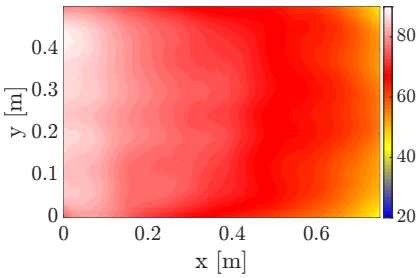

(c) Temp. distribution at $t = 900\,[sec]$

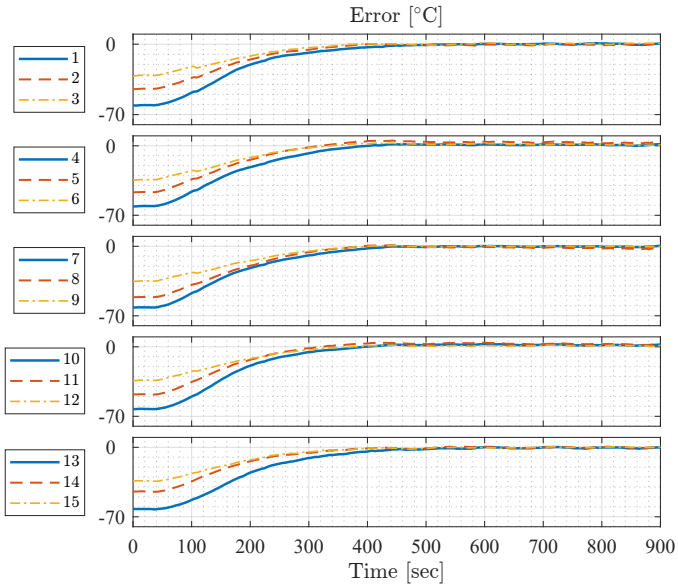

(d) Error signals for the nonuniform reference temp. distribution.

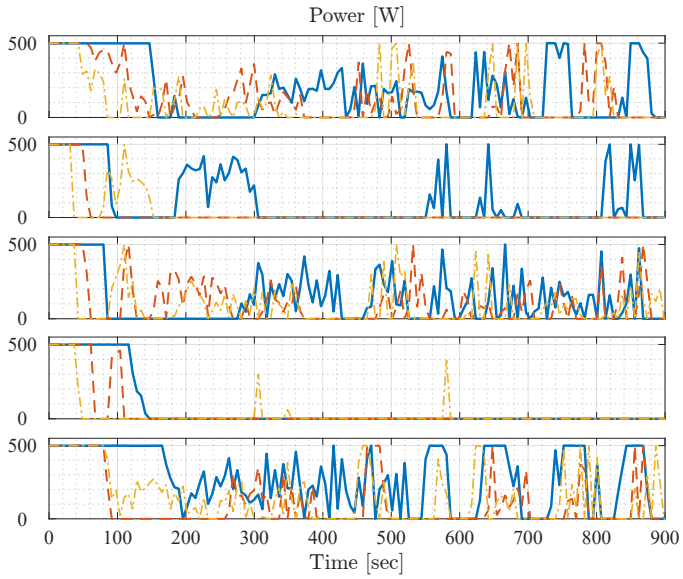

(e) Input signals for the nonuniform reference temp. distribution.

Fig. 10: Experimental results of the proposed method applied on the lab-scale thermoforming system: measured by the IR camera.

TABLE V: Overall comparison of the simulation and experimental results for the non-uniform reference temperature distribution.

Metric	Simulator	Experimental
Zones' average error [°C]	0.6	1
Zones' maximum error [°C]	±2.6	±3.8
Overshoot [°C]	0.5	5.3
Settling time (sec)	380	308

TABLE VI: A comparison between proposed MPC and Multi-agent DRL experimental results for non-uniform reference temperature distributions.

Metric	Multi-agent DRL	Proposed MPC
Average error [°C]	1.6	**1**
Maximum error [°C]	±4	**±3.8**
Overshoot [°C]	11.5	**5.3**
Settling time within an error band of ±10 °C [sec]	**236**	308

11.5°C in the multi-agent DRL method to 5.3°C in the proposed MPC, although the multi-agent DRL exhibits a shorter settling time.

VI. Conclusion

This work proposed an indirect data-driven predictive-based control method for thermal control in the thermoforming process. It outperformed state-of-the-art methods while benefiting from well-established tools and theories of system identification and linear predictive control. Several simulation studies were conducted using a high-fidelity simulator to evaluate the proposed method's robustness and performance under parametric uncertainty. The results indicated an overshoot and average steady-state error of less than 2°C and 0.9°C for the nominal scenario, and 7°C and 2°C for the worst-case scenario. Moreover, the experimental results of the proposed controller closely matched the simulation analysis, with overshoot and average steady-state error metrics of 5.3°C and 1°C, respectively.

The proposed robust linear model predictive controller design using approximate control-oriented models [32], [30], [33] is scalable and maintains performance over a wide range

of uncertainty, indicating its applicability to industrial settings. By integrating a data-driven NARX model within the linear MPC framework, we address the critical challenges associated with traditional control methods, which often struggle with thermoforming systems' dynamic and nonlinear nature. In addition, the experimental and simulation results confirmed that the proposed method outperforms more complex adaptive and learning methods in term of overheating, operation time, and steady-state errors.

For future extensions, enhanced robustness against unforeseen shifts in process dynamics can be pursued using feature-centric and automated manifold update techniques as proposed in [34]. Furthermore, we aim to explore direct data-driven control techniques that eliminate the system identification step, allowing the controller to be designed directly from the dataset. This approach has the potential to improve performance while simplifying the overall design process.

ACKNOWLEDGMENTS

We acknowledge the support of the New Frontiers in Research Fund (NFRF) of Canada, [NFRFE-2019-01440] and the Natural Sciences and Engineering Research Council of Canada (NSERC) [RGPIN-2023-03660, RGPIN-2024-05125].

REFERENCES

[1] J. L. Throne, *Technology of thermoforming*. Carl Hanser Verlag GmbH Co KG, 2013.

[2] J. P. Patil, V. Nandedkar, S. Mishra, and S. K. Saha, "Transient thermal analysis of close pressure thermoforming process," *Journal of Manufacturing Processes*, vol. 62, pp. 513–522, 2021.

[3] P. Boisse, N. Hamila, and A. Madeo, "Modelling the development of defects during composite reinforcements and prepreg forming," *Philosophical Transactions of the Royal Society A: Mathematical, Physical and Engineering Sciences*, vol. 374, no. 2071, p. 20150269, 2016.

[4] H. Hosseinionari, M. Ramezankhani, R. Seethaler, and A. S. Milani, "Development of a computationally efficient model of the heating phase in thermoforming process based on the experimental radiation pattern of heaters," *Journal of Manufacturing and Materials Processing*, vol. 7, no. 1, p. 48, 2023.

[5] Z. Albadawi, B. Boulet, R. DiRaddo, P. Girard, and V. Thomson, "Agent-based control for thermoforming processes," *IFAC Proceedings Volumes*, vol. 39, pp. 465–470, 2006.

[6] F. Borrelli, A. Bemporad, and M. Morari, *Predictive Control for Linear and Hybrid Systems*. Cambridge University Press, 2017.

[7] Z.-Z. Li, G. Ma, D.-J. Xuan, S.-Y. Seol, and Y.-D. Shen, "A study on control of heater power and heating time for thermoforming," *International Journal of Precision Engineering and Manufacturing*, vol. 11, pp. 873–878, 2010.

[8] M. M. I. Chy, B. Boulet, and A. Haidar, "A model predictive controller of plastic sheet temperature for a thermoforming process," in *2011 American Control Conference (ACC)*, 6 2011, pp. 4410–4415.

[9] H. Hosseinionari and R. Seethaler, "The integration of model predictive control and deep reinforcement learning for efficient thermal control in thermoforming processes," *Journal of Manufacturing Processes*, vol. 115, pp. 82–93, 2024.

[10] I. Jalilvand, A. M. Soufi Enayati, H. Hosseinionari, R. Seethaler, A. Narayan, B. Gopaluni, and A. S. Milani, "A multi-agent transfer reinforcement learning for adaptive digital twinning of thermoforming heating systems to enhance productivity and minimize energy consumption," 2024, available at SSRN: https://ssrn.com/abstract=5166951.

[11] H. Hosseinionari, R. Seethaler, R. J. Krishnamurthy, I. Jalilvand, and A. S. Milani, "A scalable multi-agent deep reinforcement learning in thermoforming: An experimental evaluation of thermal control by infrared camera-based feedback," *Journal of Manufacturing Processes*, vol. 131, pp. 312–326, 2024.

[12] M. Ramezankhani, M. Harandi, R. Seethaler, and A. S. Milani, "Smart manufacturing under limited and heterogeneous data: a sim-to-real transfer learning with convolutional variational autoencoder in thermoforming," *International Journal of Computer Integrated Manufacturing*, vol. 37, no. 1-2, pp. 18–36, 2024.

[13] J. Richalet, "Industrial applications of model based predictive control," *Automatica*, vol. 29, no. 5, pp. 1251–1274, 1993.

[14] Y. Zhu, "Multivariable process identification for MPC: the asymptotic method and its applications," *Journal of Process Control*, vol. 8, no. 2, pp. 101–115, 1998.

[15] Y. Zhu, R. Patwardhan, S. B. Wagner, and J. Zhao, "Toward a low cost and high performance MPC: The role of system identification," *Computers & Chemical Engineering*, vol. 51, pp. 124–135, 2013.

[16] K. Seel, E. I. Grøtli, S. Moe, J. T. Gravdahl, and K. Y. Pettersen, "Neural network-based model predictive control with input-to-state stability," in *2021 American Control Conference (ACC)*, 2021, pp. 3556–3563.

[17] N. Mohd and N. Aziz, "Control of bioethanol fermentation process: NARX-based MPC (NARX-MPC) versus linear-based MPC (lMPC)," *Chemical Engineering Transactions*, vol. 45, pp. 1297–1302, 2015.

[18] F. Bonassi, J. Xie, M. Farina, and R. Scattolini, "An offset-free nonlinear MPC scheme for systems learned by neural NARX models," in *2022 IEEE 61st Conference on Decision and Control (CDC)*, 2022, pp. 2123–2128.

[19] A. Nikolakopoulou and R. D. Braatz, "Polynomial NARX-based nonlinear model predictive control of modular chemical systems," *Computers & Chemical Engineering*, vol. 177, p. 108272, 2023.

[20] Z. Hu, J. Fang, R. Zheng, M. Li, B. Gao, and L. Zhang, "Efficient model predictive control of boiler coal combustion based on NARX neutral network," *Journal of Process Control*, vol. 134, p. 103158, 2024.

[21] W. J. Lee, J. Na, K. Kim, C.-J. Lee, Y. Lee, and J. M. Lee, "NARX modeling for real-time optimization of air and gas compression systems in chemical processes," *Computers & Chemical Engineering*, vol. 115, pp. 262–274, 2018.

[22] R. Eini and S. Abdelwahed, "Learning-based model predictive control for smart building thermal management," in *2019 IEEE 16th International Conference on Smart Cities: Improving Quality of Life Using ICT & IoT and AI (HONET-ICT)*, 2019, pp. 038–042.

[23] H. Jung and J. H. Lee, "Flexible operation of post-combustion co2 capture process enabled by NARX-MPC using neural network," *Computers & Chemical Engineering*, vol. 179, p. 108447, 2023.

[24] J. Xie, F. Bonassi, and R. Scattolini, "Learning control affine neural narx models for internal model control design," *IEEE Transactions on Automation Science and Engineering*, 2024.

[25] L. R. Schmidt, *Biaxial stretching of heat-softened plastic sheets*. University of Colorado at Boulder, 1972.

[26] CMS SpA, "CNC machining centers and thermoforming for plastics," https://www.cms.it/en_US/plastic.

[27] Q. Zhang, "Using wavelet network in nonparametric estimation," *IEEE Transactions on Neural Networks*, vol. 8, no. 2, pp. 227–236, 1997.

[28] J. B. Rawlings, D. Q. Mayne, and M. Diehl, *Model predictive control: theory, computation, and design*. Nob Hill Publishing Madison, WI, 2020, vol. 2.

[29] S. Fu, H. Sun, Z. Liu, H. Han, and Y. Zhang, "Model predictive control for nonlinear systems with two-time scales," *IEEE Transactions on Automation Science and Engineering*, vol. 21, no. 4, pp. 5088–5098, 2024.

[30] M. G. Forbes, R. S. Patwardhan, H. Hamadah, and R. B. Gopaluni, "Model predictive control in industry: Challenges and opportunities," *IFAC-PapersOnLine*, vol. 48, no. 8, pp. 531–538, 2015.

[31] O. Nelles, Nonlinear system identification, 2nd ed. Springer Nature, Sep. 2022.

[32] H. Hjalmarsson, "From experiment design to closed-loop control," *Automatica*, vol. 41, no. 3, pp. 393–438, 2005.

[33] A. Dutta, E. Hartley, J. Maciejowski, and R. De Keyser, "Certification of a class of industrial predictive controllers without terminal conditions," in *53rd IEEE Conference on Decision and Control (CDC)*, 2014, pp. 6695–6700.

[34] S. Schär, S. Marelli, and B. Sudret, "Surrogate modeling with functional nonlinear autoregressive models (F-NARX)," *Reliability Engineering & System Safety*, vol. 264, p. 111276, 2025.